

Development of Nanoparticle Stabilized Polymer Nanocontainers with High Content of the Encapsulated Active Agent and Their Application in Water-Borne Anticorrosive Coatings

Martin F. Haase, Dmitry O. Grigoriev, Helmuth Möhwald, and Dmitry G. Shchukin*

The development of the nanocontainers with the controlled uptake and release properties, proper size and shell robustness, high loading capacity and multifunctionality opens the avenue for future smart materials for drug delivery systems, feedback active surfaces and coatings, medicine and energy-enriched materials. Depending on the nature of the sensitive components (e.g., weak polyelectrolytes, metal nanoparticles) introduced into the container shell, reversible and irreversible changes of the shell permeability can be induced by various stimuli: variation of the pH, ionic strength, temperature, ultrasonic treatment, alternating magnetic field, electromagnetic fields.^[1] In general, nanocontainers (considering their shell stability and versatility of the shell modification) can be fabricated by three general approaches. The first one is based on self-assembly of amphiphilic block copolymers into spherically closed nanostructures followed by cross-linking to stabilize the nanocontainer shell.^[2] The second procedure comprises layer-by-layer assembly of oppositely charged species on the outermost surface of dense template nanoparticles using polyelectrolytes, conductive polymers, biopolymers, halloysites, carbon nanotubes, viruses, lipid vesicles, and nanoparticles as constituents of the nanocontainer shell.^[3,4] The third approach involves the use of the ultrasonic waves to fabricate inorganic and composite hollow nanospheres.^[5] However, most of the currently presented nanocontainers show quite low loading capacity and lack of multifunctionality and universality.

The surface of the reservoirs must provide colloidal stability in this environment, and also the encapsulated inhibitor molecules have to remain inside. Miniemulsion polymerization is a well known method for the fabrication of monodisperse submicron-sized latex particles and has been shown to be a technique suitable for the encapsulation of dyes, metal complexes, pigments, inorganic and liquid materials.^[6] The stabilization of the monomer droplets does not necessarily have to be done by surfactants. Solid particles can be used as stabilizing material.^[7] which is advantageous since for high particle aggregation efficiencies no additional cleaning of the polymerized product is required.

One of the nanocontainer applications is the design of the self-healing anticorrosion coatings.^[8,9] Different approaches have been published, ranging from polyelectrolyte complexes,^[10] mesoporous materials,^[11,12] layered double hydroxides,^[13,14] halloysite,^[15,16] to carbon nanotubes.^[17,18] Of particular interest for applications are inhibitor filled reservoirs that can be fabricated in a simple manner, which comprises of only few assembly steps and do not require many auxiliary materials. After fabrication the reservoirs must be transferred to the resin formulation, which consists of monomers or curable pre-polymers dissolved or emulsified in a solvent.^[19]

In a previous paper we have introduced the surface modification of silica nanoparticles by 8-hydroxyquinoline (8HQ) for its encapsulation into micron-sized nano-SiO₂ stabilized emulsion droplets.^[20] Here, we have advanced this approach for developing silica armored polystyrene (PS) composite nanocontainers (based on the Pickering emulsions) filled with 5, 10, or 20 wt% of 8HQ. The aim of our work is to introduce a new type of the containers based on Pickering emulsions as one of the delivery and controlled release tool for further application for uptake and release of the potentially various types of active materials in both delivery systems and multifunctional feedback active coatings. The approach was employed in model self-healing anticorrosion coatings in order to demonstrate the application potential of the proposed new type of the nanocontainers.

This approach fulfills the aforementioned requirements for anticorrosive coatings by applying silica-PS-8HQ composite nanocontainers in a water-based alkyd resin. Such environmentally friendly water-borne coatings have significant drawbacks concerning lower anticorrosive barrier properties compared to traditional solvent borne coatings. The present type of the nanocontainers based on Pickering emulsions is also extendable for the encapsulation of other organic corrosion inhibitors like mercaptobenzothiazole (MBT) or benzotriazole (BTA). Contrary to 8HQ, the inhibitors MBT and BTA are not soluble in styrene but the addition of a small fraction of 4-vinylpyridine (4VP) allows for their solubilization. Especially the idea of multifunctional container components is crucial for this work, since it allows for a reduction of the fabrication steps and involved reagents for their synthesis.

A bulk polymerization of styrene containing 20 wt% 8HQ yields a transparent solid (room-temperature). Gel-permeation-chromatography (GPC) shows no change of the averaged molecular mass of PS in the presence of 8HQ (see Table 1SI in Supporting Information Section). Thus, 8HQ remains molecularly

Dr. M. F. Haase, Dr. D. O. Grigoriev,
Prof. Dr. H. Möhwald, Dr. D. G. Shchukin
Max Planck Institute of Colloids- and Interfaces
Am Muehlenberg 1, 14476 Potsdam, Germany
E-mail: dmitry.shchukin@mpikg.mpg.de



DOI: 10.1002/adma.201104687

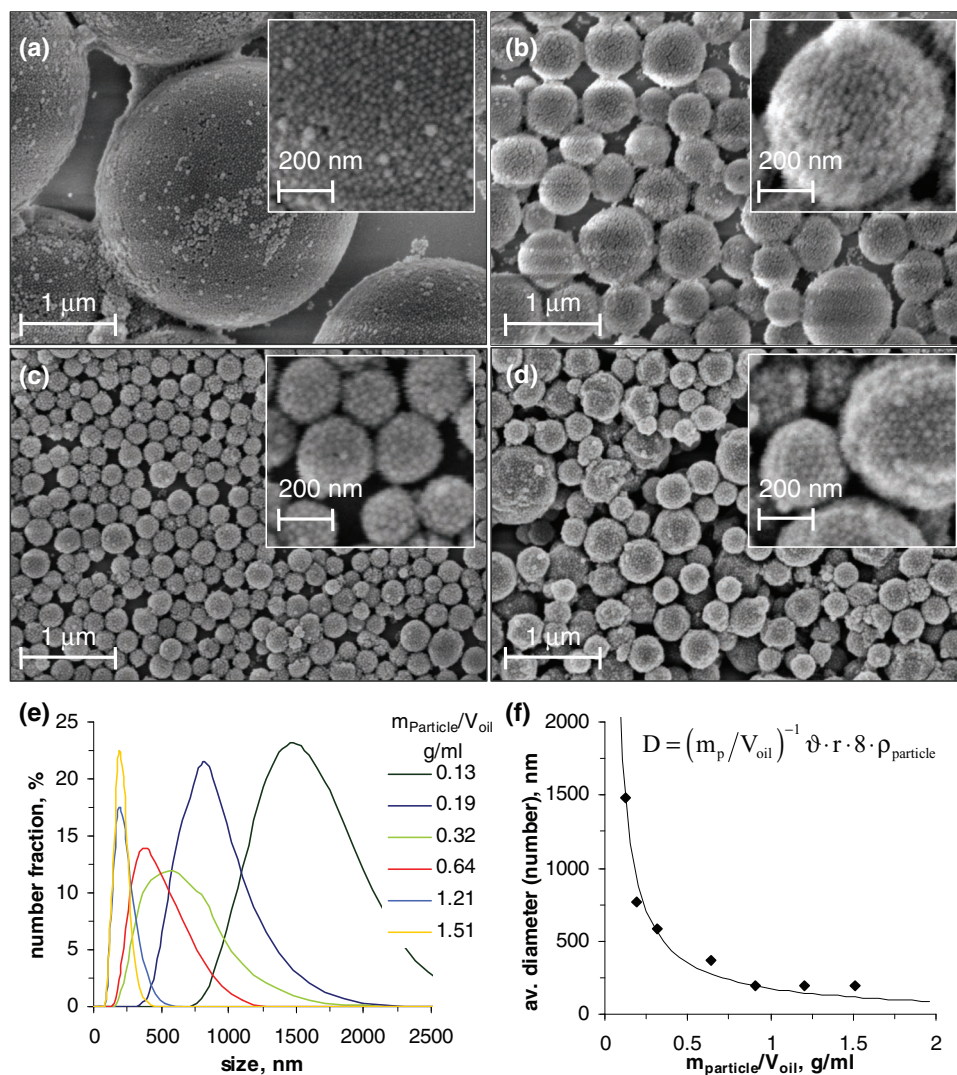


Figure 1. SEM micrographs of silica-PS-8HQ composite nanocontainers for different silica-mass to oil-volume ratios ($m_{particle}/V_{oil}$) (a) 0.09, (b) 0.32, (c) 0.91 g mL⁻¹. (d) - silica-PS-4VP-MBT composite nanocontainers (0.91 g mL⁻¹). (e) - size distributions (silica-PS-8HQ) at different silica-mass to oil-volume ratios measured by DLS. (f) number averaged diameter (silica-PS-8HQ) vs. silica-mass to oil-volume ratio, continuous line represents the calculation according to the inset formula where ϑ -hexagonal packing factor (0.907), r -silica particle radius (20 nm), $\rho_{particle}$ -silica particle density (2.2 g mL⁻¹).

dissolved in the PS matrix and does not significantly disturb the polymerization process.

SEM visualizations of silica-PS-8HQ and silica-PS-4VP-MBT composites prepared by ultrasonication are shown in **Figure 1a-d**. The shape of the polymer-silica composite nanocontainers is spherical and their size lies in the colloidal range. The composite nanocontainer shell consists of densely packed silica nanoparticles. By varying the silica nanoparticle mass fraction, the composite nanocontainer size (**Figure 1e**) can be easily controlled and decreased to a minimum of around 200 nm. The aggregation efficiency of the nanoparticles (fraction of silica attached to the polymer composites) is almost 100%, since no excess silica particles could be found in solution. By considering the surface area required for the nanoparticles to assemble densely on monodisperse droplets, a formula can be

derived (see SI) to predict the droplet size (see inset formula **Figure 1f** and continuous line).

8HQ crystals have been found in the aqueous phase after polymerization for composite nanocontainers below 3 μm, which is probably a result of Ostwald ripening. Measurements of the 8HQ release kinetics by UV-vis spectroscopy revealed a fast release (during few minutes) of the complete incorporated amount of 8HQ irrespective to the composite nanocontainer size into aqueous solution (see Supporting Information Section), which is important for further application of nanocontainers. On the contrary, the amount of 8HQ inside the reservoirs can not be dissolved in the alkyd formulation of the selected anticorrosion coating. Therefore, the composite particles allow for transferring a high amount of 8HQ in the form of highly dispersed reservoirs. Transferring e.g. 8HQ crystals

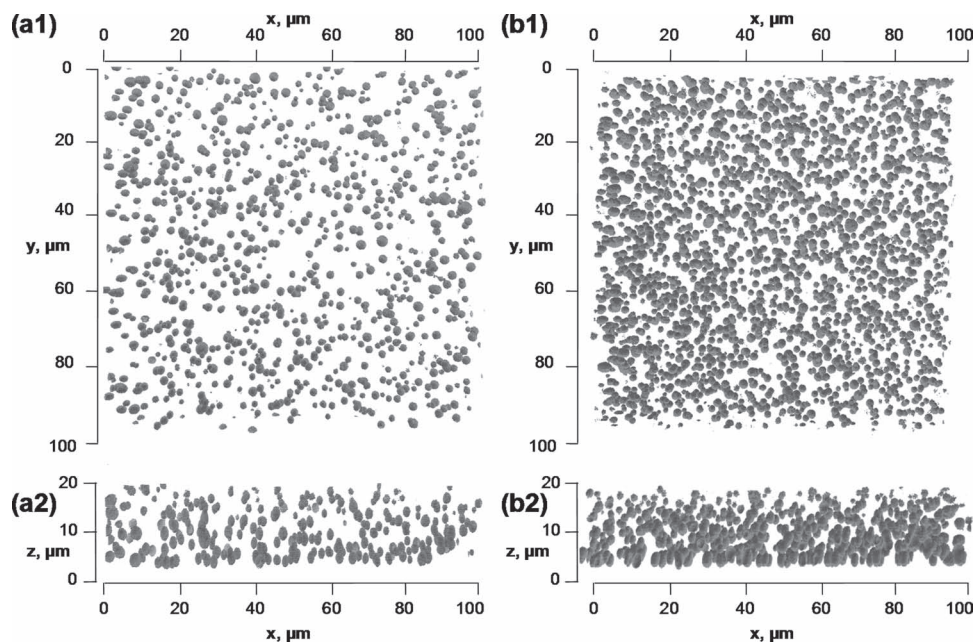


Figure 2. CLSM microscopy images of silica-PS-8HQ composite nanocontainers ($m_{\text{particle}}/V_{\text{oil}} = 0.09 \text{ g mL}^{-1}$) in a dry alkyd film on a microscope slide: (a1) and (b1) top-view, (a2) and (b2) side-view. (a) corresponds to 5 wt% and (b) to 10 wt% of silica-PS-8HQ composite nanocontainers in the dry film. The side view reaches only $25 \mu\text{m}$ into the y -direction to prevent overcrowding. Important to recognize is that the coordinate $z = 0$ does not exactly represent the surface of the substrate.

to the resin would lead to a very inhomogeneous distribution of those in the film since these crystals have neither colloidal dimension nor stability. Moreover, direct introduction of the pure inhibitor with subsequent drying results in the osmotic pressure within the film followed by coating blistering.

For the application of the composite nanocontainers in a polymeric anticorrosive coating a suitable resin must provide compatibility between the solvent and the composite nanocontainers. Organic solvent based resins tend to dissolve the composite core materials. Water based epoxy resins are cross linked by alkaline amine hardeners, which leads to dissolution of the amphoteric corrosion inhibitors. Water based alkyd resins, which are cross-linked at neutral pH simply by oxidation in air and which provide excellent dispersibility for the composite nanocontainers, fulfill these requirements. The transfer of the synthesized silica-PS-inhibitor composite nanocontainers into the alkyd coating can be performed directly from the suspension or from the dried powder of the nanocontainers by the dispersion with a rotor-stator mixing device (Ultra-Turrax). A three-dimensional visualization of fluorescence dye filled silica-PS-8HQ composite nanocontainers in a cured alkyd film, done by confocal scanning laser microscopy (CLSM), is shown in **Figure 2**.

The nanocontainers are well dispersed in the film. Examining **Figure 2(a2)** and **(b2)** can be seen that the nanocontainer concentration is increased at $z \approx 5 \mu\text{m}$. This can be interpreted as a result of sedimentation during the film drying (the nanocontainer size here is around $1\text{--}3 \mu\text{m}$). The film thickness, derived from the micrographs, is approximately $15 \mu\text{m}$. In the side view of **Figure 2** the nanocontainers appear egg-shaped, which results from the “fluorescence-shadow” that the nanocontainers

show by scanning vertically through the sample. In fact the nanocontainers are spherical as shown in **Figure 1a-d**. On the contrary, the CLSM images of the defected coatings (coatings with agglomerated nanocontainers) demonstrate either on big agglomerate or several smaller ones (results not shown).

For the evaluation of the anticorrosive properties of alkyd-coatings containing silica-PS-8HQ nanocontainers, electrochemical impedance spectroscopy (EIS) can be used. The analysis of the measured frequency dependent impedance with a model of an equivalent electrical circuit allows for the extraction of physical parameters like a specific resistance and capacitance of the films.^[21] According to the previous reports,^[13] the impedance spectra of the intact coating at small immersion times can be adequately fitted using the equivalent circuit that includes only one time constant representing the coating (**Figure 4SI**), where CPE_{coat} —Constant Phase Element for coating and $R_{\text{el, coat}}$ —Resistance of supporting electrolyte and coating, correspondingly. **Figure 3** shows impedance measurements performed during a period of 10 days, which are displayed as Bode- or Nyquist-plots.

While in **Figure 3a** the green curves represent a film with highly dispersed silica-PS-8HQ nanocontainers, the red curves represent the effect of aggregated nanocontainer domains, which generate the defects, in the film. Defects result from insufficiently dispersing the 8HQ-loaded nanocontainers in the water-based resin. This can be prevented by increasing the dispersion time and the agitating speed. On the first day both films have approximately the same values of the impedance. With time the impedance of the defect-free coating increases. Visually, the film with defects showed small black spots on its surface after 2 days of immersion in 0.1 M NaCl, which grew

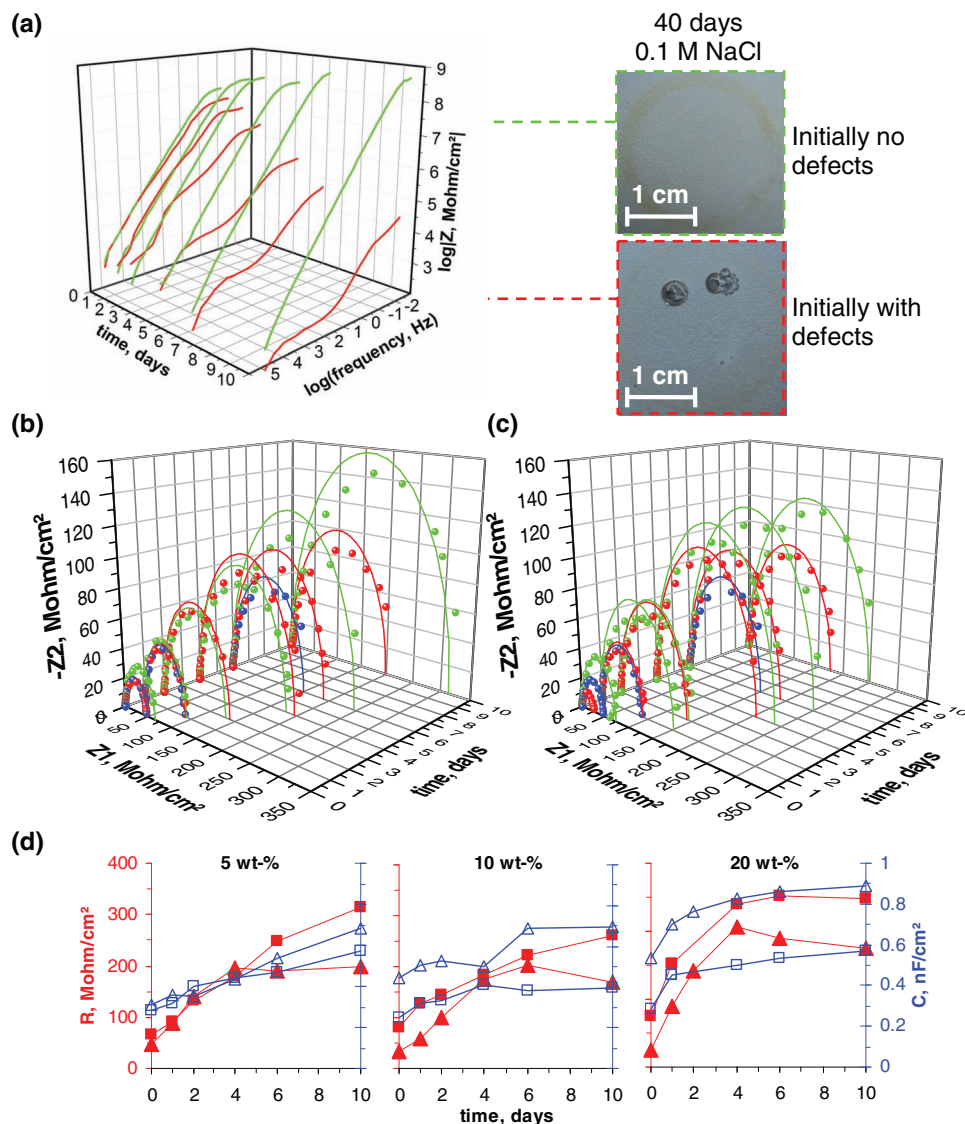


Figure 3. (a) - comparison of the impedance evolution (Bode-plot) with time of a coating with defects (containers are agglomerated, red) and a homogeneous defect-free coating (containers are homogeneously distributed, green) with both 10 wt% silica-PS-8HQ nanocontainers. (b), (c) - Nyquist plots (at 0.1 Hz) of coatings containing 5 (b) and 20 wt% (c) silica-PS nanocontainers without (red) and with (green) 8-hydroxyquinoline. Blue curves represent the blank coating. Points represent measured and continuous lines modelled impedance curves. (d) - ohmic resistance (R) and capacitance (C_1) of an alkyd polymer-film with different mass fractions of silica-PS nanocontainers on aluminium with (■) and without 20 wt% (▲) 8HQ in the composites.

in size with time (lower inset photo Figure 3a). In these spots electrochemical corrosion of aluminium takes place and, in the impedance measurements, they act as conductive areas in the coating decreasing the overall impedance of the coating. The increase of the black colored areas around the defects with time indicates so called pitting corrosion with growing creepage areas around, which denotes the corrosion below the film of alkyd polymers. The metal surface without a coating corrodes drastically in short periods of time, the impedance is in the range of MOhms and the frequency dependence of the impedance would follow a completely different trend. The defect free film did not change its morphology over the whole period of 10 days (or even 40 days, upper inset photo Figure 3a). From the visual inspection and the electrochemical measurements

it can be concluded, that the film containing the 8-HQ doped silica-PS nanocontainers not yet completely demonstrate the improvement of the EIS characteristics of the nanocontainer-loaded film, but showed promising trend in the performance improvement.

The Nyquist plots in Figure 3b and 3c show the evolution of the impedance with time for different mass-fractions of composite nanocontainers in defect free films (with the absence of agglomeration). The impedance increases with time. This could be explained by the additional cross-linking of unsaturated bonds in the fatty acid moieties of the film. The films with silica-PS nanocontainers exhibit higher impedance after 6 days as compared with the blank films. Here, the nanocontainers could act as barrier pigments decreasing the transport of charges

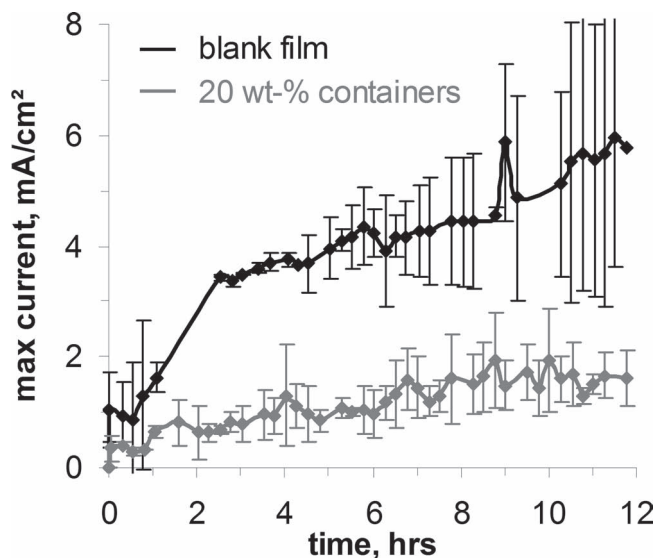


Figure 4. Maximum current densities obtained by SVET measurements for scratched alkyd coatings on aluminium in 0.1 M NaCl solution. Blue: blank coating (no nanocontainers), red: coating with 20 wt% of silica-PS-8HQ nanocontainers.

through the film. However, interesting is the observation, that the films with 8HQ doped silica-PS nanocontainers have higher impedances than the films containing silica-PS nanocontainers without 8HQ. There might be an additional passivation on the aluminium surface due to the release of 8HQ inside the microcracks of the coating. It should be recognized here also that the impedance of the alkyd films is of the same magnitude for all mass-fractions of silica-PS-8HQ.

The measured data was modeled with an equivalent parallel circuit^[13,22] that includes only one time constant representing the coating (Figure 4 in SI). The agreement of the model with the measurement is reasonable; deviations might be due to non-ideality. The parameters R and C obtained from the numerical fitting procedure are plotted in Figure 3e with dependence of time. As already recognized in the Nyquist-plots the resistance R of all polymer-films increases with time. Remarkable is the increase of R during 10 days for all mass fractions of silica-PS-8HQ capsules in the film by a factor of 3–4.

Scanning vibrating electrode measurements indicate a decreased rate of corrosion in scratches of silica-PS-8HQ doped films (Figure 4). The damage was introduced by scratching the film with a scalpel. For all samples visual changes in the form of black and white areas in the scratch were observed after 12 h. This indicates the formation of anodic and cathodic areas, as especially the white color indicates the precipitation of the corrosion product Al_2O_3 on the cathodic area. Figure 4 shows the maximum current densities, obtained by SVET measurements above the scratch area. As can be seen for all samples, maximum current densities different from zero can be observed indicating the formation of an anodic area in the scratch. However, the highest current densities are found for the blank coating, while the addition of 10 wt% silica-PS-8HQ nanocontainers to the coating seems to lower the current density in average and a further reduction can be observed by

increasing the mass-fraction of silica-PS-8HQ to 20 wt%. So, the self-repairing inhibiting effect of the impregnated -PS-8HQ is obvious for 8-hydroxyquinoline loaded at 20 wt%. The anodic current is around 0.1 after 12 h of immersion in 0.1 M aqueous sodium chloride.

The aim of our work was to introduce a new type of the containers based on Pickering emulsions, which are more flexible in preparation as previous ones and could be employed as multifunctional one-pot carrier system for different delivery and release purposes. On the basis of the hydrophobization of silica nanoparticles with 8-hydroxyquinoline (8HQ), particle stabilized emulsions of styrene containing 20 wt% of the corrosion inhibitor 8HQ in water were fabricated and subsequently polymerized to obtain silica-polystyrene-8HQ composite nanocontainers. By increasing the silica nanoparticle concentration, the size of the composite nanocontainers can be lowered down to 200 nm. The same could be achieved for an oil-in-water emulsion with the dissolved corrosion inhibitor mercaptobenzothiazol (MBT) in order to fabricate silica-poly(styrene-co-4vinylpyridine)-MBT composite nanocontainers.

An important advantage compared to the other types of the previously described nanocontainers is the very good dispersibility of the composites since their outer surface has the properties of pure silica. Separate loading or adsorption step is not required for the composites described in our work, since the inhibitor is dissolved in the initial styrene oil phase. Furthermore, it is guaranteed that the inhibitor (8-hydroxyquinoline) remains inside the reservoirs after being transferred to the resin formulation since the aqueous phase of the resin formulation does not provide sufficient solubility to dissolve the huge amounts of inhibitors inside the carriers.

Anticorrosion self-healing coatings were chosen as a model example for the demonstration of the performance of such a container type. The advantages of the presented containers in anticorrosion applications are: (i) Since this approach has been developed especially for environmental friendly water borne coatings a new direction compared to previous publications has been taken. (ii) The fabrication procedure allows also for a control over the nanocontainer size, which has not been shown for other approaches. (iii) The content of inhibitors in the composites (20 wt%) is higher than in previously reported works. Additionally, the results of the SVET measurements showed very nice self-healing effect and corrosion suppression in the damaged area for the coating with the Pickering nanocontainers. Ongoing research is focused on studying different combinations of encapsulated active agents (e.g. cathodic and anodic corrosion inhibitors) in one system like feedback active coating, which promises in the future a broad application of such a multifunctional approach.

Experimental Section

Miniemulsions with silica nanoparticles: Emulsions were always prepared with Ludox TMA particles and 13.5 wt% of the styrene monomer mixtures. The mass fractions of the components for the styrene monomer solutions are: 0.771 of styrene, 0.20 of 8HQ, 0.041 of hexadecane (HD), 0.008 of azo-bis-(isobutyronitrile) (AIBN) and for the styrene-4VP monomer solutions: 0.514 of styrene, 0.257 of 4-VP, 0.18 of MBT, 0.041 of HD, 0.008 of AIBN. A nitrogen flow was passed through

the monomer mixtures and the aqueous particle suspension for 5 min. The aqueous suspension contained sufficient NaOH or HCl to adjust the pH value for the styrene-4VP-MBT emulsion to pH 8 and for the styrene-8HQ emulsion to pH 5.0. No interaction between PS formulation and methylbenzothiazole or benzotriazole inhibitors was observed at preparation conditions. Emulsification was done by ultrasonication with a sonotrode (VCX 505, Sonics & Materials Inc. Newton, USA, 20 kHz, 40 W, 10 mm tip-diameter) for 120 s. Nitrogen gas was passed through the emulsion during emulsification. Polymerization of the emulsions took place in closed glass vials and was done in an oil bath at 65 °C for 24 h. The polymerized miniemulsions were centrifuged at 70 °C. For composite particles with 0.09 g_{Silica}/mL_{Oil}, the RPM were 3000 min⁻¹; for composites with higher silica mass contents than 0.19 g_{Silica}/mL_{Oil}, centrifugation was done at 10000 min⁻¹. The temperature maintenance during the centrifugation is required due to the problem that at 65 °C more 8-HQ or MBT is dissolved in water and cooling the aqueous phase to room temperature leads to the precipitation of this material and, thereby, contamination of the polymer-capsules. The sediment was directly added to the water-borne alkyd resin and dispersed with an ultraturax mixer at 10000 min⁻¹ for several minutes. The viscous dispersion was allowed to stand for 12 h so that air bubbles (introduced during dispersing) could ascend.

Aluminium plate pre-treatment and dip-coating: Aluminium alloy AA2024 (4.5% copper, 0.6% manganese, 1.5% magnesium) was employed as a substrate for corrosion studies. For cleaning and generating a homogeneous oxide layer on the top, aluminium plates were subjected to the following procedure: (i) Immersion into hot (60 °C) 1 M NaOH solution for 15 min, (ii) rinsing with water, (iii) immersion into (room-temperature) 15 wt% HNO₃, (iv) rinsing with deionized water and (v) drying with a nitrogen flow. A dip-coating apparatus (Siemens LOGO, 12/24RC) was used for coating of the Al plates with the water-based resin. Plates were immersed vertically into the resin for 60 s. Film formation was performed at a pull-out speed of 0.3 mm/s. The plates were then dried for 4 days in a horizontal alignment.

Electrochemical impedance measurements: In a typical EIS experiment, the sample substrates (6 cm × 3 cm) were placed into specially made cells so that 4 cm² of coated metal surface was exposed to the salt solution (approx 40 mL) and loosely covered to reduce evaporation whilst still permitting oxygen to enter the system. This allowed the simultaneous measurement of EIS alongside a long-term corrosion test. Into the cell were placed both the reference (saturated calomel) and counter (platinum) electrodes and leads attached to a clean area of the metal substrate (coating was removed using sandpaper). Measurements were carried out inside a Faraday tent using a CompactStat Impedance analyzer (Ivium technologies) at constant voltage amplitude of 10mV in a frequency range of 65 × 10³ – 10⁻² Hz (5 frequencies per decade) Where possible, data were fitted to equivalent cell diagrams as discussed in the main paper using the IviumSoft program.

SVET measurements: The characterization of the self-healing behaviour of aluminium substrates coated with alkyd coating and coating with nanocontainers was performed via the scanning vibrating electrode technique (SVET, Applicable Electronics). The vibration frequency was set to 837 Hz to achieve high response celerity. The Pt-blackened electrode tip had a diameter of 20 μm and a capacitance of 6.6 nF. The vibration amplitude was 60 μm. The electrode was held at 300 μm above the sample during the scan. The aluminum plates were fixed on a glass holder and immersed into 0.1 M sodium chloride solution. At this concentration, the specific conductivity of NaCl is 0.01 Ω⁻¹·cm⁻¹. An area of 3 mm × 3 mm was exposed while the remaining surface was covered by a sticky film. The current density was detected with a resolution of 150 μA which results in a 21 × 21-matrix. The integration time for each point was 0.5 s. A complete surface scan required less than 5 min. The analysis of the SVET data was carried out via home-made software examining the time development of minimal and maximal current densities. The damage was introduced by scratching the film with a scalpel.

Confocal Laser Scanning Microscopy: The fluorescence dye Nil red was dissolved in styrene (1 wt% Nil red, 20 wt% 8-HQ) and subsequent emulsification and polymerization yielded fluorescent dye filled polymer spheres. These nanocontainers were dispersed in a water-based alkyd-emulsion and one side of a microscopic glass slide was coated with the dispersion by dip-coating. CLSM was performed with a Leica TCS SP2 microscope. For the fluorescence excitation a laser with a wavelength of 488 nm was used, while the fluorescence light was observed in the wavelength interval 550–650 nm. The used objective had a magnification of 100× and a numerical aperture of 1.4. For the vertical scan through the polymer film a step size per image acquisition of 0.1 μm was used.

Supporting Information

Supporting Information is available from the Wiley Online Library or from the author.

Acknowledgements

We kindly thank the Worlée Chemie GmbH (Hamburg, Germany) for supplying the resin specimen. Dmitrya Borisova is acknowledged for SEM measurements. The research was supported by the ForMaT program of the German Ministry for Education and Research (BMBF) and DAAD exchange program with Portugal.

Received: December 7, 2011
Published online: April 4, 2012

- [1] A. S. Angelatos, B. Radt, F. Caruso, *J. Phys. Chem. B*, **2005**, *107*, 3071.
- [2] S. Förster, T. Plantenberg, *Angew. Chem. Int. Ed.* **2002**, *41*, 689.
- [3] G. Schneider, G. Decher, *Nano Lett.* **2004**, *4*, 1833.
- [4] D. Fix, D. V. Andreeva, Y. M. Lvov, D. G. Shchukin, H. Möhwald, *Adv. Funct. Mater.*, **2009**, *19*, 1720.
- [5] D. G. Shchukin, H. Möhwald, *Phys. Chem. Chem. Phys.*, **2006**, *8*, 3496.
- [6] K. Landfester, C. K. Weiss, in *Modern Techniques for Nano- and Microreactors/Reactions*, Vol. 229, Springer-Verlag Berlin, Berlin **2010**, 1.
- [7] a) F. Tiarks, K. Landfester, M. Antonietti, *Langmuir* **2001**, *17*, 5775; b) K. Zhang, W. Wu, K. Guo, J.-F. Chen, P.-Y. Zhang, *Colloids and Surfaces A* **2009**, *349*, 110.
- [8] D. G. Shchukin, H. Mohwald, *Chem. Commun.* **2011**, *47*, 8730.
- [9] *MRS Bull.* **2005**, *30*, 694.
- [10] D. O. Grigoriev, K. Kohler, E. Skorb, D. G. Shchukin, H. Mohwald, *Soft Matter* **2009**, *5*, 1426.
- [11] M. J. Hollamby, D. Fix, I. Donch, D. Borisova, H. Mohwald, D. Shchukin, *Adv. Mater.* **2011**, *23*, 1361.
- [12] D. Borisova, H. Mohwald, D. G. Shchukin, *ACS Nano* **2011**, *5*, 1939.
- [13] J. Tedim, S. K. Poznyak, A. Kuznetsova, D. Raps, T. Hack, M. L. Zheludkevich, M. G. S. Ferreira, *ACS Appl. Mater. Interfaces* **2010**, *2*, 1528.
- [14] G. Williams, H. N. McMurray, *Electrochem. Solid State Lett.* **2004**, *7*, B13.
- [15] E. Abdullayev, Y. Lvov, *J. Mater. Chem.* **2010**, *20*, 6681.
- [16] D. G. Shchukin, S. V. Lamaka, K. A. Yasakau, M. L. Zheludkevich, M. G. S. Ferreira, H. Mohwald, *J. Phys. Chem. C* **2008**, *112*, 958.
- [17] M. F. Montemor, M. G. S. Ferreira, *Surf. Coat. Technol.* **2008**, *202*, 4766.

- [18] G. Lanzara, Y. Yoon, H. Liu, S. Peng, W. I. Lee, *Nanotechnology* **2009**, *20*, 7.
- [19] P. A. Sorensen, S. Kiil, K. Dam-Johansen, C. E. Weinell, *J. Coat. Technol. Res.* **2009**, *6*, 135.
- [20] M. F. Haase, D. Grigoriev, H. Möhwald, B. Tiersch, D. G. Shchukin, *Langmuir* **2011**, *27*, 74.
- [21] S. V. Lamaka, M. L. Zheludkevich, K. A. Yasakau, M. F. Montemor, M. G. S. Ferreira, *Electrochim. Acta* **2007**, *52*, 7231.
- [22] M. Taryba, S. V. Lamaka, D. Snihirova, M. G. S. Ferreira, M. F. Montemor, W. K. Wijting, S. Toews, G. Grundmeier, *Electrochim. Acta* **2011**, *56*, 4475.
-